

The Ouroboros of Memristors: Neural Networks Facilitating Memristor Programming

Zhenming Yu^{*†‡}, Ming-Jay Yang^{†‡}, Jan Finkbeiner^{*†}, Sebastian Siegel[†], John Paul Strachan^{*†}, Emre Neftci^{*†}

^{*}Fakultät für Elektrotechnik und Informationstechnik, RWTH Aachen, Aachen, 52074, Germany

[†]Peter Grünberg Institut, Forschungszentrum Jülich GmbH, Jülich, 52425, Germany

{z.yu, m.yang, e.neftci}@fz-juelich.de

[‡]These authors contributed equally to this work.

Abstract—Memristive devices hold promise to improve the scale and efficiency of machine learning and neuromorphic hardware, thanks to their compact size, low power consumption, and the ability to perform matrix multiplications in constant time. However, on-chip training with memristor arrays still faces challenges, including device-to-device and cycle-to-cycle variations, switching non-linearity, and especially SET and RESET asymmetry [1], [2]. To combat device non-linearity and asymmetry, we propose to program memristors by harnessing neural networks that map desired conductance updates to the required pulse times. With our method, approximately 95% of devices can be programmed within a relative percentage difference of $\pm 50\%$ from the target conductance after just one attempt. Our approach substantially reduces memristor programming delays compared to traditional write-and-verify methods, presenting an advantageous solution for on-chip training scenarios. Furthermore, our proposed neural network can be accelerated by memristor arrays upon deployment, providing assistance while reducing hardware overhead compared with previous works [3]–[6].

This work contributes significantly to the practical application of memristors, particularly in reducing delays in memristor programming. It also envisions the future development of memristor-based machine learning accelerators.

I. INTRODUCTION

Memristive devices have emerged as promising accelerators for machine learning and neuromorphic engineering, thanks to their compact size, non-volatility, and low latency [7]. While previous studies have showcased memristor-based inference accelerators [8], [9], less progress has been seen with on-chip training and fine-tuning. While high-precision programming of memristor conductances is attainable through write-and-verify methods, as demonstrated in [10], the extended programming delay hinders its application in on-chip learning and impedes the deployment of memristive crossbar arrays. In on-chip learning scenarios, pulses of specific duration are preferred [11]. However, non-idealities in memristors, such as non-linearity, asymmetry, device-to-device, and cycle-to-cycle variations, with update asymmetry severely impact network performance [1], [2]. Although non-ideality-aware methods and algorithms like Tiki-Taka offer solutions to mitigate these issues, they need additional steps during training and introduce extra hardware overhead [3]–[6].

Upon revisiting the method of programming memristors using predefined pulses, an intriguing observation emerges: in our efforts to program δG , we manipulate pulse time t and voltage U , which can only impact G through complex

physical dynamics. Naturally, the resulting response is neither linear nor symmetric. To effectively address the challenges posed by update asymmetry and non-linearity, what we really need is something capable of translating the desired δG into the required pulse time t . However, due to inherent noise and variations in memristors, constructing static look-up tables is challenging. To address this obstacle, we propose a novel method: training neural networks for memristor programming to map desired conductance updates to the required voltage pulses. As the switching dynamics of memristors are linked to their current conductance, the neural pulse predictor takes the current conductance G and the update ΔG as input. This symbiotic relationship, depicted in Fig. 1, where memristors accelerate the neural pulse predictor, which in turn aids in programming themselves, holds significant potential. Given that the programming pulse prediction network consistently operates in inference mode, it can be embedded onto memristor arrays through precise write-and-verify methods, producing swift prediction results while utilizing only a fraction of the hardware resources.

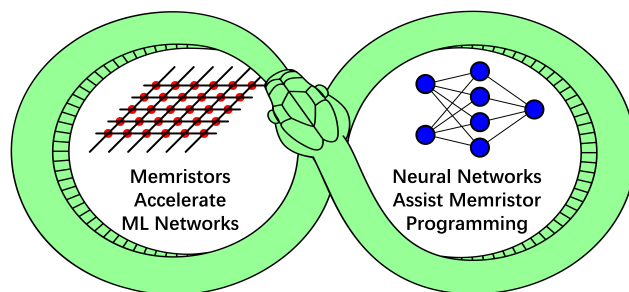


Fig. 1. The Ouroboros of Memristors: While memristors are typically utilized to bolster machine learning networks, our innovative approach leverages neural networks to streamline memristor programming, thereby amplifying on-chip training performance for upcoming memristor-based accelerators.

II. SIMULATION SETUP

A. Device Modeling

In accordance with [1], we employed the JART VCM model [12] for our simulation setup. This model was chosen for its detailed physics-driven noise mechanisms and has been experimentally validated [13]. As illustrated in Fig. 2(a), the JART model abstracts the filament region of VCM devices

as a stack, represented as circuit elements in series. Cycle-to-cycle noises were implemented as random walks in the length and radius of the filament region, as well as in the boundaries of oxygen vacancy concentration, which induces noises in the G_{\max} and G_{\min} . We adopted a simplified model [14] mathematically fitted to the JART model to streamline calculations. The simulation results are presented in Fig. 2(b).

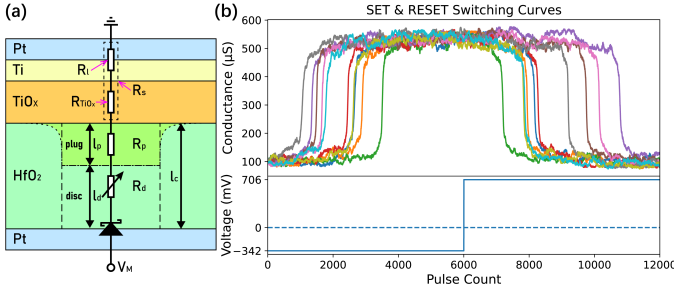


Fig. 2. (a): Illustration of the equivalent circuit diagram for the JART memristor model. (b): Simulation results depicting switching curves following the application of 6000 SET pulses and 6000 RESET pulses across 10 devices.

B. Dataset Generation

We utilized the model detailed in Sec. II-A to generate the training dataset. We selected only one pair of V_{SET} and V_{RESET} for programming the memristor. These voltages were maintained following the specifications in [1], ensuring smooth transitions and accessibility to intermediate states.

The dataset generation process begins with a random conductance G_{start} and a random target G_{target} within the operational range. We then choose to apply V_{SET} or V_{RESET} based on the direction of the target and apply the voltage for $10ns$. Cycle-to-cycle noise was introduced to the selected parameters, as explained in Sec. II-A, and the conductance was recorded. The cycle continues until the conductance before and after the time step lies on two sides of G_{target} . The conductance closer to G_{target} was selected as G_{end} , and the time for the device to switch from G_{start} to G_{end} was recorded as t_{pulse} .

It is important to note that in our simulation setup, we did not account for the conductance change during the rising and falling edges. Thus, many short pulses are equivalent to one long pulse. As we could check the device conductance at any time in simulation without disturbing the memristor state variables, we effectively have a prolonged pulse that stopped just when G_{end} was closest to G_{target} .

Given that we only used 2 applied voltages, V_{SET} and V_{RESET} , we employ the sign of t_{pulse} to denote the switching direction. If G_{target} exceeded G_{start} , V_{SET} was used, and t_{pulse} remained positive. Conversely, if G_{target} was less than G_{start} , V_{RESET} was used, and t_{pulse} was designated as negative.

We recorded the complete $G-t$ histories for a duration of $2 \times t_{\text{pulse}}$ as references during both training and validation. This process was repeated 10,000 times for the complete dataset, which was then partitioned into ratios of [80%, 10%, 10%] for training, validation, and testing, respectively.

III. NEURAL PULSE PREDICTOR

A. Network Training

We used PyTorch to construct and train our neural pulse predictor. The inputs, G_{start} and δG , as well as the output, t_{pulse} , were approximately normalized to the interval [0, 1]. Due to the cycle-to-cycle noises, the input range was not precisely defined. Therefore, we opted for a rough normalization, bringing the values to similar ranges. We designed a fully connected neural network with 3 hidden layers, configured with sizes [2 (input size), 32, 64, 32, 1 (output size)]. The Relative Percentage Difference (RPD) defined as

$$\text{RPD} = \text{mean} \left(\frac{|X_{\text{output}} - X_{\text{target}}|}{X_{\text{target}}} \right) \quad (1)$$

was used to assess the performance. The network was trained for 100 epochs using Mean Squared Error (MSE) loss between t_{output} and t_{target} . We saved networks based on their RPD on the validation dataset. Two approaches for RPD evaluation were explored: direct evaluation with t and mapping onto G . In the first approach, RPD was calculated with t_{output} and t_{target} . In the second approach, t_{output} was mapped to G_{output} using the $G-t$ histories recorded. If t_{output} fell outside the recorded range, the first or last recorded G was used as G_{output} . Subsequently, RPD was calculated using G_{output} and G_{target} .

To evaluate the network's performance, we deployed it in simulation as described in Sec. II. The network received the current conductance G_{start} and the target δG , predicting the voltage pulse needed to program G_{target} onto the memristor device. We simulated the pulse accordingly, compared G_{end} with G_{target} , and calculated RPD using Eq. 1. Additionally, we included a baseline performance calculated by utilizing the pulse time that would result in the same δG with the noise-free model unaffected by cycle-to-cycle noises.

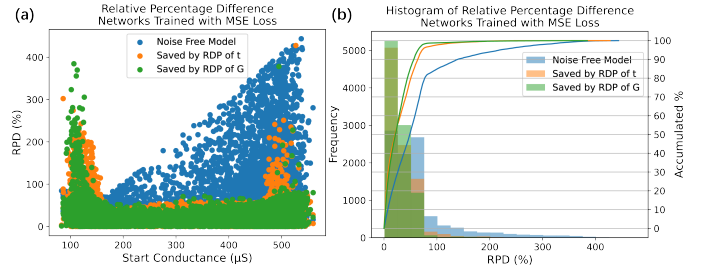


Fig. 3. (a) RPDs of G_{output} generated by networks deployed in simulation and (b) the corresponding histograms. These networks underwent training from the ground up using MSE loss. The models were saved based on the best RPD of t_{output} or G_{output} observed on the validation dataset.

The networks trained with MSE loss and saved based on the best RPD relative to t_{target} or G_{target} on the validation dataset exhibited similar performance. Both networks outperformed the baseline pulse predictor running a noise-free model, as shown in Fig. 3. Fig. 3(a) reveals a strong association between the performance of the trained models and the starting conductance. When G_{start} is in the middle of the full conductance range, the trained networks perform

well, programming G_{end} s closer to G_{target} than the noise-free baseline. However, when G_{start} is close to G_{min} or G_{max} , errors in conductance programming begin to increase.

This behavior is attributed to the memristor model described in Sec. II-A, which features two self-accelerating feedback loops in its switching dynamics. In the SET direction, the rise of conductance induces more thermal heat-up, lowering the energy barrier for device switching. In the RESET direction, the rise of resistance increases the voltage drop on the memristor device, accelerating the switching process. Both self-accelerating processes saturate when the device approaches the conductance boundaries, resulting in S-shaped switching curves shown in Fig. 2(b). As a result, the model reacts slowly to pulses when it is close to G_{min} and G_{max} . With the noise magnitude being bigger than the conductance changes, shorter pulses may not appear to have significant impacts on the recorded data. Consequently, the neural pulse predictor tends to produce larger errors when starting with conductance close to G_{min} or G_{max} .

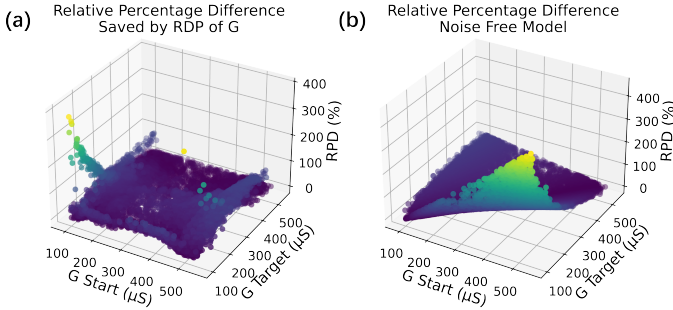


Fig. 4. RPDs plotted with G_{start} and G_{target} for the pulse predictors (a) trained from scratch with MSE loss, and (b) based on noise-free model.

A closer examination of the results, plotted with G_{target} in Fig. 4, reveals an increase in RPD at low G_{start} with the trained neural pulse predictor, but not with the noise-free baseline. This discrepancy arises because we encoded pulse directions in the sign of t_{pulse} . In regions where G_{start} is close to G_{min} , the effect of pulses in both directions is insignificant, and noise dominates the conductance change. In such cases, the trained network has a higher likelihood of predicting pulses in the wrong direction. However, the noise-free baseline is calculated using simulation and never has direction error. This provides the noise-free baseline with an advantage, allowing it to outperform the trained networks with low G_{start} .

B. Network Fine-tuning

If we look at the training method in Sec. III-A, an intriguing aspect becomes apparent. While the goal is to bring G_{end} closer to G_{target} , the networks are trained on t_{target} . While this method is both straightforward and computationally simple, it can not guarantee proximity between G_{end} and G_{target} due to the model’s highly non-linear $G - t$ transfer curve as evident from Fig. 2(b).

In light of this, an alternative approach was explored, utilizing the recorded $G - t$ histories as piecewise functions

to map t_{output} to G_{output} . The network was then trained on MSE loss between G_{output} and G_{target} . To mitigate noise in the recorded $G - t$ histories, we implemented a smoothing process using moving average filters with various kernel sizes for convolution. Customized backward function was used to mitigate non-differentiable points, and clamped the gradient to 1 to guide the output towards the recorded regions, as depicted in Fig. 5.

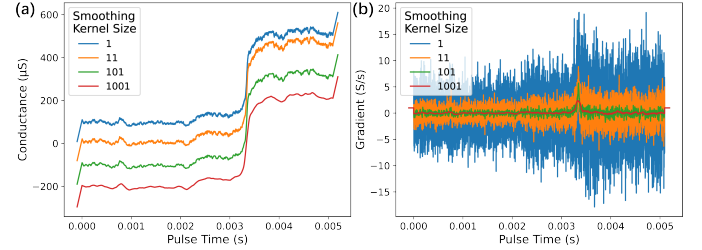


Fig. 5. (a) Mapping of $G - t$ (kernel size 11, 101, and 1001 shifted for better visibility) and (b) the corresponding gradients in an example $G - t$ history. Various kernel sizes were employed during the smoothing process.

We utilized the model from Fig. 4(a) and fine-tuned the weights. We first attempted fine-tuning without smoothing the $G - t$ histories, training the network for 100 epochs and saving the weights that produced the best match between G_{output} and G_{target} on the validation dataset for testing. Then, we experimented with smoothed $G - t$ histories by decreasing smoothing kernel sizes from 1001, 101, 11 to 1 during the training process. The network was trained with each smoothing kernel for 50 epochs, and the weights were saved based on the best RPD performance during validation. This approach aimed to address overshooting gradient descents, stabilize the training process, and enhance the overall performance, and the results are shown in Fig. 6.

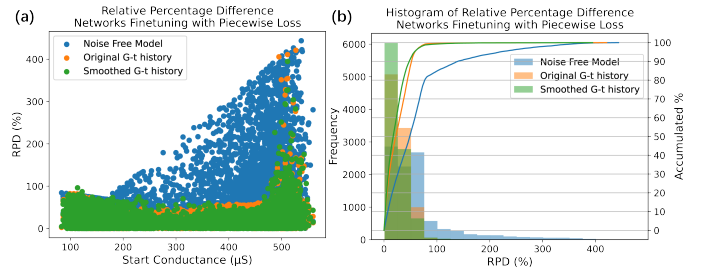


Fig. 6. (a) RPDs of G_{output} generated by various networks deployed in simulation and (b) the corresponding histograms depicting the distribution. These networks underwent fine-tuning from a model initially trained with MSE loss and were saved based on the best RPD performance observed on the validation dataset.

The fine-tuning process yielded a notable improvement in performance. By utilizing fixed gradients outside the recorded range, the output was guided toward the correct direction, resulting in performance increases at low G_{start} , matching the noise-free baseline, as shown in Fig. 6(a). Performance was further enhanced with smoothed gradients, and RPDs of less than 50% were achieved in approximately 95% of all trials.

IV. WRITE-AND-VERIFY DEMO

A. Demonstration In Simulation

To showcase the performance of our networks, we configured the memristor device to different conductances across the range and attempted to program them towards a shared G_{target} . After 10 write-and-verify iterations, most devices reached their converged conductance. The results after 20 iterations are presented in Fig. 7(a). The noise-free model faces challenges near G_{min} and G_{max} due to the self-accelerating processes discussed in Sec. III-A, resulting in its poor performance. Although it successfully converges in other regions, the simulation time is significantly extended due to intensive computations. In contrast, the model fine-tuned with piecewise $G-t$ histories achieves performance comparable to the baseline. It achieved stability with low standard deviations and aligns well with G_{target} . The model trained with MSE loss on t_{target} exhibits noisier behavior and lacks consistent convergence to G_{target} .

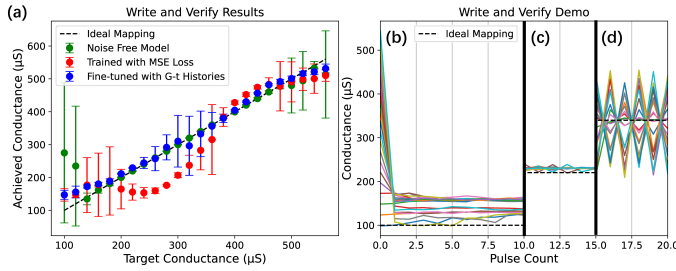


Fig. 7. (a) Converged mapping of G_{end} and G_{target} after 20 write-and-verify iterations. (b) Histories of the predictor network fine-tuned with smoothed $G-t$ of (b) $100\mu\text{S}$, (c) $220\mu\text{S}$, and (d) $340\mu\text{S}$.

For G_{target} close to the conductance boundaries, G_{end} is heavily influenced by the noise of G_{min} and G_{max} , as shown in Fig. 7(b), G_{end} stabilize slightly away from G_{target} . In regions where the network performs well, as Fig. 7(c) shows, G_{end} stay stably close to G_{target} . However, towards where the t_G transfer curve becomes sharp and the impact of noise increases, network performance starts to decline, with G_{end} overshooting and oscillating around G_{target} , as shown in Fig. 7(d).

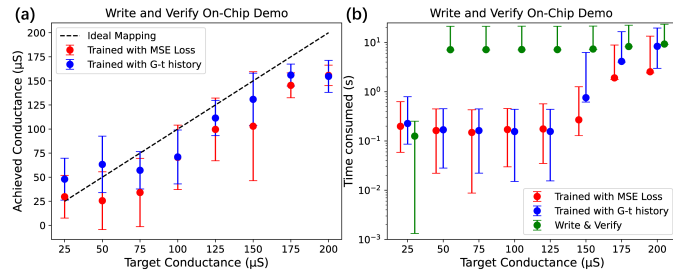


Fig. 8. On-chip demonstration of (a) converged mapping of G_{end} and G_{target} after 10 iterations. (b) comparison of programming delay for the device to converge into the window of $G_{\text{target}} \pm 50\mu\text{S}$ using different write methods.

B. On-Chip Demonstration

To demonstrate the predictor’s performance on real devices, we utilize a memristor testing system integrated with CMOS

circuitry [15]. The device characteristics were fitted with a statistical model [16], and the neural predictor was trained as outlined in Section III. The obtained results are presented in Fig. 8. Notably, the time delay for writing target conductance is significantly lower than the baseline write-and-verify method [17]. Precision performance is expected to further improve with data from models that better account for device and circuit noises, or directly from experimental measurements.

V. DISCUSSION

Poor Performance of Noise-free Model: In Sec. III-A, the noise-free baseline exhibits poor performance. The exact reason for this remains unclear, but could be linked to the switching dynamics discussed in Sec. III-A, where injected noises could further assist the self-accelerating switching processes, and introduce biases in the predictions.

Another plausible factor is the asymmetric impact of noise. As explained in Sec. II-A, the change parameters could disproportionately influence switching dynamics, causing deviations with the predictions derived from mean values.

Training with Varying Voltages: We trained the network with fixed voltages to ease the data collection. While high voltages may damage the device, prolonged pulse length can be achieved easily. In reality, precision tuning of applied voltages using a DAC is more feasible, whereas the precision of pulse length is limited to clock frequencies, and one could train networks that work with varying voltages instead.

Better Write-and-Verify Approaches: Our approach minimizes programming overhead compared to traditional algorithms. Its simplicity offers advantages on device tuning, in terms of latency and power dissipation, beneficial for on-chip training. Although this approach might have limited precision, as long as the update sign remains unchanged, the weight will eventually converge.

VI. CONCLUSION

We have introduced a novel approach to program memristor by training neural networks predicting update pulses. Our neural pulse predictor demonstrates a significant reduction in programming delay compared to traditional write-and-verify methods, particularly advantageous in applications such as on-chip training and fine-tuning. Upon deployment, the neural pulse predictor can be integrated into memristor accelerators, utilizing a minimal fraction of the available memristor arrays while predicting pulses with an $O(1)$ time complexity. Additionally, multiple networks can be trained to operate in parallel and enhance precision across various conductance ranges. Our work offers a fresh perspective on the symbiotic relationship between memristors and neural networks and sets the stage for innovation in memristor tuning optimizations.

ACKNOWLEDGMENT

This work was sponsored by the Federal Ministry of Education, Germany (project NEUROTEC-II grant no. 16ME0398K and 16ME0399). We thank Dr. Vasileios Ntinias for his help with the simplified model [14] and Dr. Stephan Menzel for his advice on the JART model noise implementations.

COPYRIGHT

© 2024 IEEE. Personal use of this material is permitted. Permission from IEEE must be obtained for all other uses, in any current or future media, including reprinting/republishing this material for advertising or promotional purposes, creating new collective works, for resale or redistribution to servers or lists, or reuse of any copyrighted component of this work in other works.

REFERENCES

- [1] Z. Yu, S. Menzel, J. P. Strachan, and E. Neftci, "Integration of physics-derived memristor models with machine learning frameworks," in *2022 56th Asilomar Conference on Signals, Systems, and Computers*, 2022, pp. 1142–1146.
- [2] C. Lee, K. Noh, W. Ji, T. Gokmen, and S. Kim, "Impact of asymmetric weight update on neural network training with tiki-taka algorithm," *Frontiers in neuroscience*, vol. 15, p. 767953, 2022.
- [3] T. Gokmen and W. Haensch, "Algorithm for training neural networks on resistive device arrays," *Frontiers in neuroscience*, vol. 14, p. 103, 2020.
- [4] T. Gokmen, "Enabling training of neural networks on noisy hardware," *Frontiers in Artificial Intelligence*, vol. 4, p. 699148, 2021.
- [5] M. Onen, T. Gokmen, T. K. Todorov, T. Nowicki, J. A. Del Alamo, J. Rozen, W. Haensch, and S. Kim, "Neural network training with asymmetric crosspoint elements," *Frontiers in Artificial Intelligence*, vol. 5, p. 891624, 2022.
- [6] M. J. Rasch, F. Carta, O. Fagbohunge, and T. Gokmen, "Fast offset corrected in-memory training," *arXiv preprint arXiv:2303.04721*, 2023.
- [7] S. Spiga, A. Sebastian, D. Querlioz, and B. Rajendran, *Memristive Devices for Brain-Inspired Computing: From Materials, Devices, and Circuits to Applications-Computational Memory, Deep Learning, and Spiking Neural Networks*. Woodhead Publishing, 2020.
- [8] M. Hu, C. E. Graves, C. Li, Y. Li, N. Ge, E. Montgomery, N. Davila, H. Jiang, R. S. Williams, J. J. Yang *et al.*, "Memristor-based analog computation and neural network classification with a dot product engine," *Advanced Materials*, vol. 30, no. 9, p. 1705914, 2018.
- [9] M. Le Gallo, R. Khaddam-Aljameh, M. Stanisavljevic, A. Vasilopoulos, B. Kersting, M. Dazzi, G. Karunaratne, M. Brändli, A. Singh, S. M. Mueller *et al.*, "A 64-core mixed-signal in-memory compute chip based on phase-change memory for deep neural network inference," *Nature Electronics*, vol. 6, no. 9, pp. 680–693, 2023.
- [10] M. Rao, H. Tang, J. Wu, W. Song, M. Zhang, W. Yin, Y. Zhuo, F. Kiani, B. Chen, X. Jiang *et al.*, "Thousands of conductance levels in memristors integrated on cmos," *Nature*, vol. 615, no. 7954, pp. 823–829, 2023.
- [11] M. J. Rasch, D. Moreda, T. Gokmen, M. Le Gallo, F. Carta, C. Goldberg, K. El Maghraoui, A. Sebastian, and V. Narayanan, "A flexible and fast pytorch toolkit for simulating training and inference on analog crossbar arrays," in *2021 IEEE 3rd international conference on artificial intelligence circuits and systems (AICAS)*. IEEE, 2021, pp. 1–4.
- [12] F. Cüppers, S. Menzel, C. Bengel, A. Hardtdegen, M. Von Witzleben, U. Böttger, R. Waser, and S. Hoffmann-Eifert, "Exploiting the switching dynamics of hfo2-based reram devices for reliable analog memristive behavior," *APL materials*, vol. 7, no. 9, p. 091105, 2019.
- [13] C. Bengel, A. Siemon, F. Cüppers, S. Hoffmann-Eifert, A. Hardtdegen, M. von Witzleben, L. Hellmich, R. Waser, and S. Menzel, "Variability-aware modeling of filamentary oxide-based bipolar resistive switching cells using spice level compact models," *IEEE Transactions on Circuits and Systems I: Regular Papers*, vol. 67, no. 12, pp. 4618–4630, 2020.
- [14] V. Ntinias, D. Patel, Y. Wang, I. Messaris, V. Rana, S. Menzel, A. Ascoli, and R. Tetzlaff, "A simplified variability-aware vcm memristor model for efficient circuit simulation," in *2023 19th International Conference on Synthesis, Modeling, Analysis and Simulation Methods and Applications to Circuit Design (SMACD)*, 2023, pp. 1–4.
- [15] C. Li, J. Ignowski, X. Sheng, R. Wessel, B. Jaffe, J. Ingemi, C. Graves, and J. P. Strachan, "Cmos-integrated nanoscale memristive crossbars for cnn and optimization acceleration," *IEEE International Memory Workshop*, 2020.
- [16] M.-J. Yang and J. P. Strachan, "State-space modeling and tuning of memristors for neuromorphic computing applications," *ICONS '23: Proceedings of the 2023 International Conference on Neuromorphic Systems*, 2023.
- [17] S. Yu, "Neuro-inspired computing with emerging non-volatile memory," *Proceedings of the IEEE*, 2018.